

# Calculation models of the electrodynamic accelerator (railgun)

**Abstract.** The analysis of phenomena occurring in the railway accelerator (railgun) has been presented in the paper. The analytical and numerical models have been used. The formulas describing the forces acting on the accelerated element (bullet) for different models of the accelerator have been derived. The dimensions of rails and bullet for each model have been assumed to be the same. In case of numerical calculations the finite element method has been used. For a chosen accelerator type the field-circuit model has been made with using MATLAB-Simulink software. The selected model has been verified experimentally.

**Streszczenie.** W artykule przedstawiono analizę zjawisk zachodzących w akceleratorze szynowym. Wykorzystano zarówno modele analityczne, jak i numeryczne. Otrzymano wzory opisujące siły działające na element przyspieszany (pocisk) dla różnych modeli akceleratora. Przyjęto identyczne wymiary szyn i pocisku dla każdego modelu. W przypadku obliczeń numerycznych wykorzystano metodę elementów skończonych. Dla wybranego typu akceleratora wykonano model polowo-obwodowy z wykorzystaniem oprogramowania MATLAB-Simulink. Model ten został zweryfikowany pomiarowo. (Modele obliczeniowe akceleratora elektrodynamicznego (działo szynowe)).

**Keywords:** electrodynamic accelerators, analytical models, numerical models, field-circuit method.

**Słowa kluczowe:** akceleratorzy elektrodynamiczne, modele analityczne, modele numeryczne, metoda polowo-obwodowa.

## Introduction

Currently, magnetic launchers are analysed in many experiments and research works [1, 2, 3, 4,]. They could be used not only in military applications [5, 6], but also covers different areas of industry [7]. However, their functioning very often causes various problems that need to be solved and eliminated in order to ensure proper operation of the device. Problems are mainly related to the necessity to deliver large currents (kA or MA) in a very short period of time of a few milliseconds.

In order to improve the electrodynamic launcher parameters, it is necessary not only to carry out experimental studies, but also to create an appropriate computational model that best fit the real device. There are several possibilities to increase thrust force without increasing supply current, through a properly designed magnetic circuit. Therefore, a correct field model allows to optimize the structure of the accelerator.

In the paper three different types of rail accelerator have been compared: ironless railgun (ILR), iron-core railgun (ICR) and iron-core permanent magnet railgun (ICPMR). For all analysed objects the analytical and numerical models have been developed. In case of analytical models only the force has been determined, while in numerical model the flux value has been calculated additionally. In the case of ICR the field-circuit model has been developed and verified experimentally.

## Analytical models of railguns

The analytical models of analysed accelerators have been derived with using different technics. In the case of ironless railgun, the Biote-Savarte law was used. In the case of ICR and ICPMR accelerators, the equivalent magnetic circuit technic was implemented.

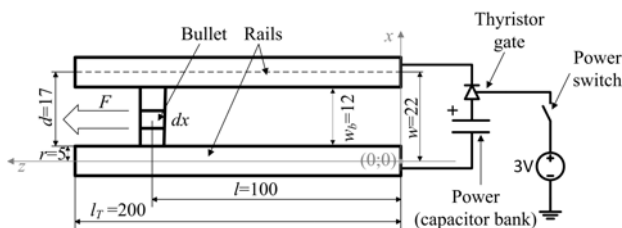


Fig.1. Simplified schematic of the ironless accelerator (dimensions in [mm]).  $l_T$  – total length of rails,  $F$  – force acting on the bullet.

## Ironless railgun

The simple outline of the ILR is shown in Fig. 1. Generally, it consists of two parallel conductors and a bullet between them. These three elements along with the capacitors form a closed circuit for the current flow.

The force arising in ILR is the Lorentz force. After closing the circuit, there is a short-circuit state and a large current flows (of the order of several or tens of kA), which excites the transverse magnetic field and acts with the current flowing in the bullet.

To calculate the magnetic field distribution in the area of the bullet, the Biote-Savarte law could be used. Using the notation in Fig. 1 we obtain:

$$(1) \quad B(x) = \frac{\mu_0 \cdot I}{4\pi x} \cdot \left( \frac{l}{\sqrt{l^2 + x^2}} \right)$$

where:  $\mu_0$  – magnetic permeability of vacuum,  $l$  – length of the current carrying rails,  $I$  – current flowing in the rails and bullet,  $x$  – distance from the zero point.

The Lorentz force acting on the bullet is described by the expression:

$$(2) \quad F = \int_r^{w-r} IBdx$$

Substituting eq. (1) in (2) we obtain (notation - see Fig. 1):

$$(3) \quad F = \frac{\mu_0 \cdot I^2}{4\pi} \cdot \left( -\ln \left( \frac{l + \sqrt{l^2 + d^2}}{d} \right) + \ln \left( \frac{l + \sqrt{l^2 + r^2}}{r} \right) + \right. \\ \left. -\ln \left( \frac{l + \sqrt{l^2 + (w-r)^2}}{w-r} \right) + \ln \left( \frac{l + \sqrt{l^2 + (w-d)^2}}{w-d} \right) \right)$$

## Iron-core railgun

The ICR is presented in Fig. 2. For calculations the reluctance network method has been used. The symmetry of the object has been assumed. The non-linear characteristic of the core has been taken into account (Fig. 3), as well.

In order to calculate the average value of the magnetic flux density in the air gap (Fig. 4), the parameters of the reluctance network have to be determined. In case of the air

gap leakage flux, the simplified analytical expression has been used (Fig. 4) [8]:

$$(4) \quad R_{\mu r} = \frac{0,17 \cdot \delta + 0,14 \cdot h_t}{\mu_0 \cdot l \cdot h_t}$$

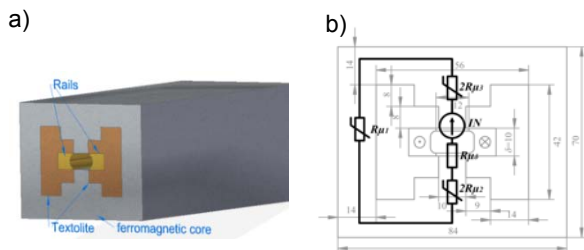


Fig. 2. The outline (a) and reluctance network (b) of the iron-core railgun [9] (dimensions in [mm])

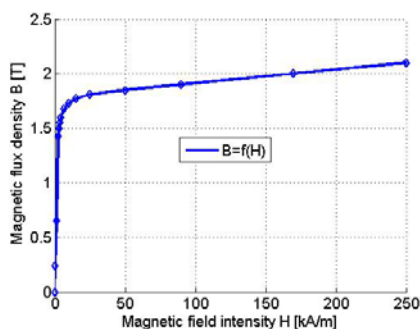


Fig. 3. B/H curve of the ferromagnetic core

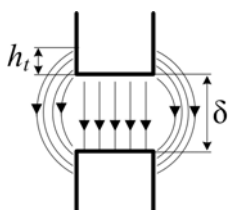


Fig. 4. The magnetic flux density in the air gap

The total air gap reluctance (including leakage flux) has been calculated using a simple expression for parallel connection of two reluctances:

$$(5) \quad R_{\mu \delta r} = \frac{R_{\mu \delta} \cdot R_{\mu r}}{R_{\mu \delta} + R_{\mu r}}$$

where:  $R_{\mu \delta}$  – reluctance of the air gap without leakage flux.

In order to obtain the flux value  $\Phi$ , the nonlinear equation has been solved:

$$(6) \quad I - R_{\mu \delta r} \Phi = (R_{\mu 1}(\Phi) + 2R_{\mu 2}(\Phi) + 2R_{\mu 3}(\Phi)) \cdot \Phi$$

where:  $\Phi$  – magnetic flux,  $R_{\mu \delta r} = 3.0607e+6$  [1/H],  $R_{\mu 1}(\Phi)$ ,  $R_{\mu 2}(\Phi)$ ,  $R_{\mu 3}(\Phi)$  – nonlinear reluctances of the magnetic circuit (Fig. 2).

The Lorentz force  $F$  has been obtained with using the formula (assuming, that vectors of flux density and current flow direction are perpendicular to each other):

$$(7) \quad F = BIw_b$$

where:  $w_b$  – approximated length of the bullet (Fig. 1),  $B$  – an average value of the magnetic flux density in the bullet obtained from the flux calculations (eq. 6).

### Iron-core permanent magnet railgun

In case of ICPMR the similar model as for the ICR has been implemented (Fig. 5). The linear parameters of the model are given in table 1. In order to obtain magnetic flux value in the bullet area, the following nonlinear equation has been solved (Fig. 5b):

$$(8) \quad R_{\mu 1}(\Phi) \cdot \Phi = I + 2H_c \cdot h_m - R_{\mu \delta} \Phi - 2 \cdot R_{\mu m} \Phi$$

where:  $R_{\mu m}$  – PM reluctance,  $H_c$  – coercivity value of the PM

Table 1. Linear parameters of the ICPMR reluctance network model

Quantity	$H_c$	$R_{\mu \delta}$	$R_{\mu m}$	$h_m$
Unit	kA/m	1/H	1/H	m
Value	890	5.305e+6	6.316e+6	0.015

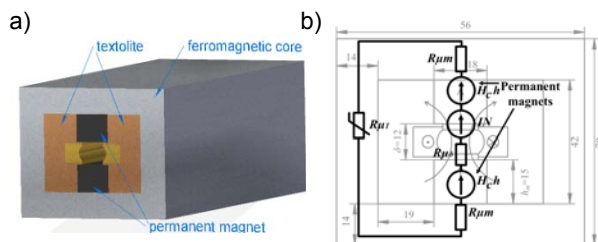


Fig. 5. The 3D view (a) and reluctance network model (b) of the ICPMR accelerator [9] (dimensions in [mm])

### Numerical models of accelerators

In the numerical calculations the ANSYS-Maxwell software has been used. The magnetostatic model with voltage excitation has been implemented. The eddy current effects has been neglected. In such a case Maxwell's equations in the following form have to be solved [10]:

$$(9) \quad \nabla \times \mathbf{H} = \mathbf{J}; \quad \nabla \times \mathbf{E} = 0; \quad \nabla \cdot \mathbf{B} = 0$$

where:  $\mathbf{H}$  – magnetic intensity vector,  $\mathbf{J}$  – current density vector,  $\mathbf{E}$  – electric intensity vector,  $\mathbf{B}$  – magnetic flux density vector.

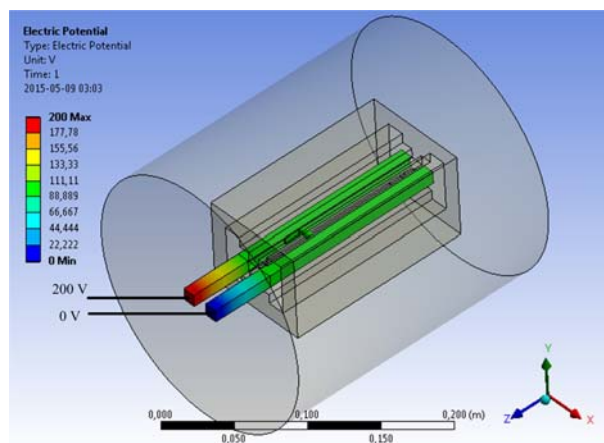


Fig. 6. Model of the ICR in ANSYS software with the voltage boundary conditions

The voltage boundary conditions have been assumed on the rails ends (Fig. 6). On the outer boundaries the zero Dirichlet condition was assumed. The discretization mesh has been chosen after some numerical experiments and is a compromise between calculation time and accuracy.

Magnetic flux calculations have been performed for different positions of the projectile and different values of the excitation current. The flux passing through a surface  $S$  (limited by a bullet and rails) can be calculated as:

$$(10) \quad \Phi = \int_S \mathbf{B} \cdot \mathbf{n} dS$$

where:  $\Phi$  - flux enclosed by the bounding surface  $S$ ,  $\mathbf{B}$  - flux density vector,  $\mathbf{n}$  - unit normal vector.

The force acting on the bullet is numerically integrated using the expression:

$$(11) \quad \mathbf{F} = N \int_{\Omega} (\mathbf{J} \times \mathbf{B}) d\Omega$$

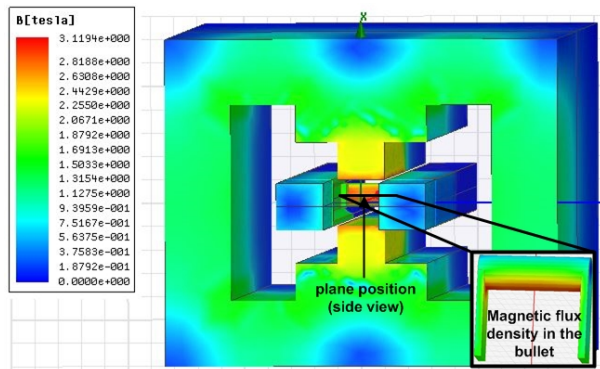


Fig.7. Magnetic flux density in the ICR cross section for  $U=200$  V

In Fig. 7 an example of the magnetic flux density distribution for  $U=200$  V has been depicted. The current value in rails reaches 19.5 kA. The magnetic flux density highest value is observed in the bullet area and in the tooth area of the iron core. The magnetic field distribution in the bullet is highly non-homogenous – it varies between 0.7 T (front of the bullet) and 3 T (back of the bullet).

### Calculation results

Calculations have been carried out for current values  $I=1\div 20$  kA. Analytical models have been compared with numerical ones.

Table 2. Calculation results for thrust

Type of accelerator	Forced current	Force (analytical)	Force (numerical)
	kA	N	N
ILR	20	110.75	130.60
	10	27.70	32.65
	1	0.28	0.33
ICR	20	290.38	322.54
	10	90.36	88.88
	1	1.65	0.89
ICPMR	20	418.68	350.45
	10	166.16	153.09
	1	12.73	9.93

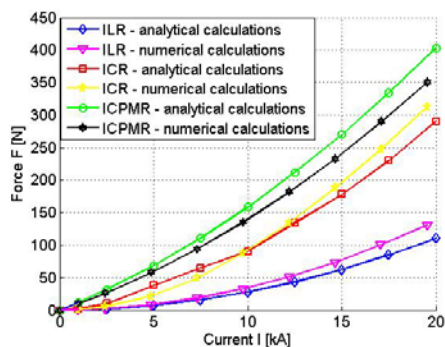


Fig.8. Force vs. current values for different models and accelerator constructions

In table 2 the force for three chosen current values have been compared. In Fig. 8 waves of thrust vs. current for numerical and analytic models are compared. The absolute differences between analytical and numerical models increase along with the increasing of current value. It is due to simplification of the analytical models (simplified expression for leakage reluctance value, assumption of homogenous current distribution in rails and bullet, simplified magnetic field distribution in bullet area). However, differences do not exceed 20%, which means that presented analytical models could be used in introductory designing of accelerators.

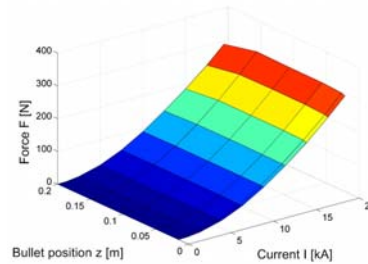


Fig.9. Thrust characteristic for ICR

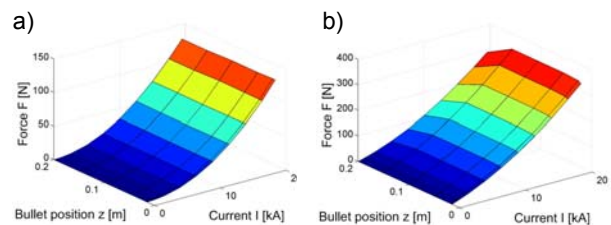


Fig.10. Thrust characteristics for: a) ILR, b) ICPMR

In Figs. 9-10 characteristics of thrust vs. current value and bullet position for different accelerator constructions are given. They have been obtained with using numerical models. The force value depends insignificantly on the bullet position and is rising exponential vs. current value. For investigated current values range, the highest thrust is observed for ICPMR accelerator construction. For  $I=20$  kA it is about 2.7 times higher comparing to ILR. The thrust increases fastest vs. current value in case of ICR. It means, that for current value above 20 kA, this type of accelerator could reach higher thrust than the ICPMR.

### Transient model of the ICR

In case of accelerators not only static, but also dynamic parameters are important. In the paper, the transient model of ICR has been created. A field-circuit method was implemented. Equations describing the dynamic model of the railgun have been formulated based on the Euler-Lagrange's method:

$$(12) \quad \frac{dv}{dt} = \frac{F(i, x) - Dv}{m}; \quad \frac{dx}{dt} = v$$

$$(13) \quad \frac{di}{dt} = \frac{-Ri - \frac{d}{dx}(\Phi(i, x))v - \frac{q}{C}}{\frac{d}{di}\Phi(i, x)}$$

where:  $v$  – bullet velocity,  $D$  – friction coefficient,  $m$  – mass of the bullet,  $R$  – circuit resistance,  $q$  – electric charge,  $C$  – capacitance.

Equations 12 describe the mechanical part of the system, while the eq. 13 describes the electrical part. Equations above have been implemented in the MATLAB–Simulink software. The thrust and flux characteristics (obtained from numerical field calculations) have been included in the form of Look-up tables (Figs. 9 and 11). In table 3 constant parameters of the model have been given.

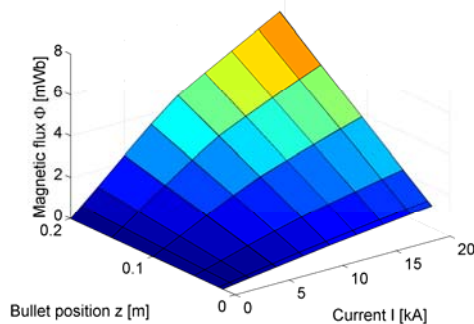


Fig.11. The magnetic flux vs. current value and bullet position

Table 3. Constant parameters of the field-circuit model

Friction coefficient	$D$	Ns/m	0.35
Mass of the bullet	$m$	[kg]	0.00556
Resistance	$R$	[mΩ]	7.6
Length of the bullet	$d_b$	[m]	0.0296
Inductance of the supply circuit	$L_s$	[μH]	2

#### Measurement verification of the ICR transient model

The bullet velocity and current waves have been verified experimentally. In order to determine the bullet velocity, the optical gate has been used. It is characterized by 5 ns response time. The current waves have been measured indirectly, with using the resistor (0.517 mΩ) and an oscilloscope (10 bit resolution, 40 ns sample time).

Table 4. Measurement and calculations results (100 mF)

$U_c$	$I_{max}$	$\Delta t$	$v_{meas}$	$v_{calc}$
[V]	[A]	[ms]	[m/s]	[m/s]
210	18878	1.007	29.43	30.8
160	14235	1.953	15.23	14.03

In case of bullet velocity a good conformity between calculation and measurement results is observed (Table 4). The differences do not exceed 8%. In case of current waves there are some slightly differences observed between calculation and experimental results (Fig. 12). The measured current wave increases more rapidly. It could be due to simplification of the supply circuit model (e.g. the delays have been neglected). The maximum current value is proportional to the capacitor voltage.

#### Conclusion

There are only relatively small differences between thrust calculations with using analytical and numerical models. Thus, the presented analytical models can be used in the designing of railguns.

In case of field-circuit model, there is observed a good agreement between calculation and measurement results both for bullet velocity and for current waves. The differences are mostly due to the simplification of the mathematical model as well as measurement system accuracy. The investigations have shown, that the calculation results are very sensitive to friction coefficient and inductance values. The mathematical and physical models will be improved in future researches.

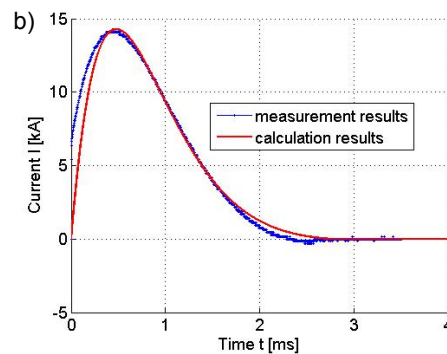
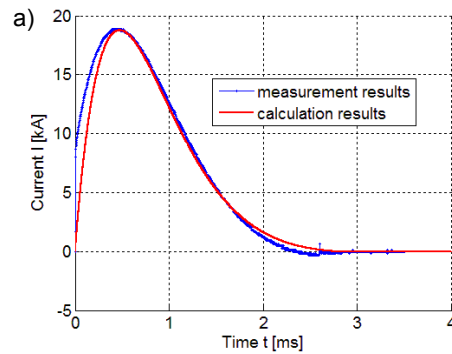


Fig.12. Current waves vs. time for: a)  $U=210$  V and  $C=100$  mF, b)  $U=160$  V and  $C=100$  mF

**Autorzy:** dr hab. inż. Andrzej Waindok, Politechnika Opolska, Katedra Elektrotechniki Przemysłowej, ul. Proszkowska 76, 45-758 Opole, E-mail: [a.waindok@po.opole.pl](mailto:a.waindok@po.opole.pl); mgr inż. Paweł Piekielny, Katedra Elektrotechniki Przemysłowej, Politechnika Opolska, ul. Proszkowska 76, 45-758 Opole, E-mail: [p.piekielny@po.opole.pl](mailto:p.piekielny@po.opole.pl)

#### REFERENCES

- Waindok A., Mazur G., Mutual Inductances in a Mathematical Model of the Three-Stage Reluctance Accelerator, *Proceedings of the IIIrd International Students Conference on Electrodynamics and Mechatronics (SCE III)*, Opole, Poland, October 6-8, (2011), 115-118.
- Domian J., Kluszczyński K., Hybrid pneumatic-electromagnetic – general concept, mathematical model and results of simulation, *Przegląd Elektrotechniczny*, 89 (2013), nr.12, 21-25.
- Mikołajewicz J., Analiza stanów pracy kaskadowej wyrzutni elektromagnetycznej na podstawie połowego modelu zjawisk, *Przegląd Elektrotechniczny*, 82 (2006), nr.12, 20-23.
- Beach F.C., Design and Construction of a One Meter Electromagnetic Railgun, *Master's thesis*, Naval Postgraduate School Monterey CA, USA, June 1996.
- Jin L., Lei B., Zhang Q., Zhu R., Electromechanical Performance of Rails With Different Cross-Sectional Shapes in Railgun, *IEEE Trans. on Plasma Science*, 43 (2015), n.5, 1220-1224.
- Xing Y.C., Lv Q.A., Lei B., et al., Analysis of Transient Current Distribution in Copper Strips of Different Structures for Electromagnetic Railgun, *IEEE Trans. on Plasma Science*, 43 (2015), n.5, 1566-1571.
- Lehmann P., Reck B., Vo M. D., Behrens J., Acceleration of a Suborbital Payload Using an Electromagnetic Railgun, *IEEE Trans. on Mag.*, 43 (2007), n.1, 480-485.
- Gieras J.F., Piech Z.J., Tomczuk B., Linear synchronous motors, Taylor & Francis, USA, (2012).
- Waindok A., Piekielny P., Analysis of Selected Constructions of the Electrodynamic Accelerator, *International Symposium on Electrodynamics and Mechatronic Systems (SELM)*, Zawiercie, Poland, May 15-18, (2013), 51-52.
- Kohnke P., ANSYS Mechanical APDL Theory Reference, November (2013).